

RESEARCH

Open Access



Experimental Analysis and Evaluation of the Compressive Strength of Rubberized Concrete During Freeze–Thaw Cycles

Sheng Sun^{1,4}, Xiaoyan Han^{1*} , Aijiu Chen¹, Qing Zhang^{2,3}, Zhihao Wang¹ and Keliang Li¹

Abstract

Recycling scrap tires provides an alternative source of fine aggregates for the production of rubberized concrete and this will lead to significant increase in concrete frost resistance, environmental protection, and conservation of natural sand and gravel resources. In this paper, a total of 25 groups of rubberized concrete were produced by adding scrap tire rubber particles of different sizes, contents, and pretreatment methods to replace the fine aggregate, and their compressive strength during freeze–thaw cycles was studied from both the macro- and meso-perspectives. The results indicated that the decrease in concrete strength and weight was notably restricted by the presence of rubber particles during freeze–thaw cycles. The rubber fine aggregate with smaller particle sizes enhanced the concrete frost resistance more significantly, and the F_{100} of concrete with rubber particles of 1.0–2.0 mm increased from 76.6 to 86.5% by increasing the rubber content from 0.0 to 5.6%. The effects of rubber fine aggregate on concrete compressive strength during freeze–thaw cycles were quantified. On this basis, a forecast model for rubberized concrete compressive strength in freeze–thaw cycles was proposed, and the effects of the particle size, content, and pretreatment of the rubber particles were considered. The calculated results agreed well with the test results both in this study and the relevant peer studies, indicating that the model can provide a good reference for the design and engineering application of rubberized concrete in frigid environments.

Keywords Compressive strength, Rubberized concrete, Mesostructure, Freeze–thaw cycles, Forecast model

1 Introduction

The recycling of tires as alternative materials for concrete production (Guo et al., 2017; Pham et al., 2019; Torretta et al., 2015) is of great significance for environmental protection and improvement of concrete frost resistance. Recent years have witnessed scientific research achievements, and some substantive progress has been made in this application (Han, 2020; Pacheco-Torres et al., 2018; Siddika et al., 2019). The preliminary engineering application of rubberized concrete in the Hekou Reservoir and Qianping Reservoir water control projects in Henan Province, China, showed that rubberized concrete had satisfactory improvements in crack resistance, dynamic resistance, abrasion resistance, and frost resistance, and presented potential

Journal information: ISSN 1976-0485 / eISSN 2234-1315

*Correspondence:

Xiaoyan Han
little1216@163.com

¹ North China University of Water Resources and Electric Power, School of Civil Engineering and Communication, Zhengzhou 450011, People's Republic of China

² State Key Laboratory Hydrology Water Resources & Hydraulic Engineering, Hohai University, Nanjing 210098, Jiangsu, People's Republic of China

³ Department of Mechanical Engineering, Hohai University, Nanjing 210098, Jiangsu, People's Republic of China

⁴ China Railway NO.3 Engineering Group Co. Ltd, Beijing, China

engineering applications (Wang et al., 2018; Yuan et al., 2017 [HYPERLINK "sps:refid::bib47|bib49"](#)).

The rubber surface pretreatment improved the strength and durability of the rubberized concrete. It has been proven that the addition of rubber particles significantly deteriorates the physical and mechanical properties of concrete regardless of rubber size or shape (Assaggaf et al., 2022; Li et al., 2016; Yu & Zhu, 2016). The compressive strength of rubberized concrete decreased by 24.0% when 10.0% of the fine aggregates were replaced, and the reduction was larger when the coarse aggregates were replaced (Gesoglu et al., 2014; Jafari & Toufigh, 2017; Rahman et al., 2013; Xie et al., 2019). The pretreatment of the rubber with sodium hydroxide solution and silane coupling agent significantly improved rubberized concrete strength and uses the advantages of other properties, such as the deformation adaptability, crack resistance, frost resistance, etc. (He et al., 2018; Li et al., 2019). Pelisser et al. (2011) reported that the compressive strength of concrete with 10.0% rubber particles pretreated with sodium hydroxide was only 14.0% lower than that of the reference group, and the flexural strength was improved by 30.0% by pretreating the rubber particles with a silane coupling agent.

The addition of the appropriate amount and particle size of rubber particles significantly improved the frost resistance of concrete. Gong et al. (2018) and Pham et al. (2019) reported that the rubberized cement-based materials were more resistant under freeze–thaw environments than the control one, and the rubberized concrete aged for 5 years still exhibited better frost resistance than normal concrete. Grinys et al. (2020) and Richardson et al. (2012) have reported that some scholars suggested that the rubber content of 5.0% by volume provided noticeable air entrainment to concrete, and the rubber particle in size of 0.00–1.00 mm and volume of 3.5% concrete was similar to that of air-entraining concrete. In addition, the optimum content and size of the rubber particles providing maximum freeze–thaw protection and maximum strength were 1.4% and less than 0.5 mm, respectively (Richardson et al., 2012, 2016). Zhang et al. (2006) reported that the center distance of rubber powder with a size of 0.14 mm for concrete with 2.0–4.0% rubber content was 330–660 μm and larger than the recommended value of air-entrained concrete, whose effects on concrete compressive strength and frost resistance were equivalent to those of the air-entraining agent. The frost resistance of rubberized concrete may be further enhanced by the strengthened rubber–cement matrix interface and the reduction of adhesion defects by pretreating the rubber particles (Grinys et al., 2020; Pham et al., 2019).

The deformation adaptability, failure state, and bearing capacity of concrete after freeze–thaw cycles changed to varying degrees compared with the normal group (Dvorkin, 2019; Hu & Wu, 2019; Huda & Alam, 2015; Pilehvar, 2019). With the increase in freeze–thaw cycles, the concrete deformation corresponding to the same stress increased (Liu & Wang, 2012), and the concrete specimens with freeze–thaw damage failed in a brittle manner (Berto et al., 2015). The degradation model of concrete strength under freeze–thaw cycles established by Zhu et al. (2009) and Zhao et al. (2017) provided important references for the evaluation of freeze–thaw damaged concrete properties and promoted the development of research on concrete damage. However, the addition of rubber particles has been shown to enhance the concrete frost resistance, buffer the sudden change in concrete stiffness and internal force during compression (Xu et al., 2020), and significantly affect the concrete strength in freeze–thaw cycles. Therefore, using the existing model of normal concrete, it is difficult to accurately describe the evolution of the strength of rubberized concrete with freeze–thaw cycles.

As mentioned above, considerable achievements in the frost resistance of rubberized concrete obtained in the existing studies have expedited the development of rubberized concrete. Meanwhile, some deficiencies exist at the present stage. First, the mechanism of freeze–thaw damage for rubberized concrete under the effects of rubber content and pretreatment remains to be further clarified. Second, methods for calculating the compressive strength of rubberized concrete in freeze–thaw cycles that consider the effects of the rubber content and the pretreatment, and the evolution law of compressive strength for rubberized concrete with freeze–thaw cycles remains to be further studied. Therefore, it is necessary to study and evaluate the compressive strength of rubberized concrete in freeze–thaw cycles.

In this paper, two kinds of rubber particles with different sizes were pretreated with sodium hydroxide solution, and the cubic compressive strength of concrete mixed with these rubber particles in freeze–thaw cycles was studied. The mechanism of freeze–thaw damage for rubberized concrete under the effects of rubber content and pretreatment was analyzed. Finally, a predictive model of compressive strength for rubberized concrete in freeze–thaw cycles was proposed.

2 Experimental Design

2.1 Materials and Concrete Mixes

The materials used to produce the specimens included Grade 42.5 ordinary Portland cement, river sand and crushed stone in continuous grading 0.00–4.75 mm and 5.00–20.00 mm as the fine and coarse aggregates,

respectively, rubber particles in sizes of 1.00–2.00 mm and 2.00–4.00 mm obtained by crushing waste tires.

The physical and chemical properties of the cement are listed in Table 1. The water absorption and specific gravity of fine aggregate were 1.3% and 2.58, and that of the coarse aggregate were 1.0% and 2.70. The specific gravity of the rubber particles was 1.25, and the rubber content, ash content, fiber content and moisture content were 51.2%, 2.7%, 0.5% and 0.6%, respectively. The particle size distribution for the rubber fine aggregate, river sand and crushed stone is shown in Fig. 1. Sodium hydroxide solutions with mass concentrations of 5.0% and 10.0% were used to pretreat the rubber particles. The physical properties, mechanical properties, particle size distributions of the materials mentioned above and the pretreatment method for rubber particles have been reported in a parallel study on dynamic properties of rubberized concrete (Chen et al., 2021).

The concrete mixes were designed based on China Standards JGJ 55–2011 (2011). The concrete (C0) without rubber particles was used as the reference group. The rubber particles were added to the concrete by replacing 5.0%, 10.0%, 15.0% and 20.0% of the fine aggregate in equal volumes, and the rubber contents were 1.4%, 2.8%, 4.2% and 5.6%, respectively, by volume of concrete. A total of 25 groups of concrete mixtures, including the reference concrete and the rubberized concrete with untreated rubber particles and pretreated rubber particles, and their nomenclature and mixing proportions are listed in Table 2.

2.2 Specimens and Test Method

The 100-mm concrete cubes containing a larger surface area were more vulnerable to damage than the 150-mm concrete cubes (Richardson et al., 2012). Therefore, the 100-mm concrete cubes were designed as the specimens for this test based on China Standard GBT50082-2009 (2009) and ASTM C666/C666 M-15 (2015). The 3 specimens of each group, making a total of 15 (3 × 5), were tested for the properties of concrete after 0, 25, 50, 75 and 100 freeze–thaw cycles (5 groups). A total of 375 (15 × 25) specimens for the 25 kinds of concrete listed in Table 2 were produced. The specimens were demolded one day after concrete pouring and then

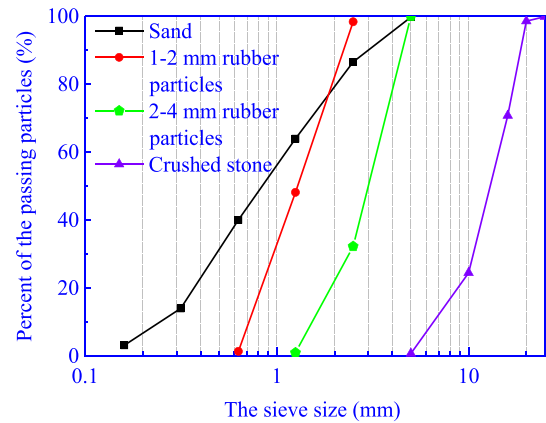


Fig. 1 Gradation curves of the sand, rubber particles and crushed stone

transferred and stored in a curing room maintained at 20 ± 5 °C and 95% relative humidity for 27 days, being saturated with water for the last 4 days.

The fresh concrete slump and air content were tested in strict accordance with the methods for Test of Slump and Test of Air Content in China Standard GB/T50080-2016 (2016). As shown in Fig. 2, CDR-5 automatic freeze–thaw test equipment and a WHY-2000 servo loading machine were used to perform tests on fast freeze–thaw cycles and compressive strength of concrete according to the fast freeze–thaw experimental design listed in Table 3. The concrete air-void structure analyzer shown in (Fig. 2c) was used to determine hardened concrete air-void parameters based on the method of straight-line traverse in Standard SL352-2006 (2006).

The mass loss rate (W_n) and relative compressive strength (F_n) were determined by Eq. (1) and Eq. (2), respectively:

$$W_n = \frac{G_0 - G_n}{G_0} \times 100\%, \tag{1}$$

$$F_n = \frac{f_{cu,n}}{f_{cu0}} \times 100\%, \tag{2}$$

where f_{cu} and G are the cube compressive strength and the mass of the specimens, respectively, and the

Table 1 Physical and mechanical properties of the cement

Setting time (min)		Compressive strength (MPa)		Flexural strength (MPa)		Density (kg/m ³)	Blaine fineness (m ² /kg)	Loss on ignition (%)
Initial	Final	3 days	28 days	3 days	28 days			
180	250	25.70	49.60	4.80	7.90	3100.00	348.30	1.05

Table 2 Mixing proportion

Mix	Rubber size	Rubber (%)			Sand (kg/m ³)	Stone (kg/m ³)	Cement (kg/m ³)	Water (kg/m ³)	Slump (mm)	Air (%)
		Un-treated	5% NaOH	10% NaOH						
C0		0.0			728.0	1092	325	180	60	2.2
R ₁₋₂ C1	1-2 mm	1.4			692.6	1092	325	180	57	2.8
R ₁₋₂ C2	1-2 mm	2.8			655.2	1092	325	180	55	3.0
R ₁₋₂ C3	1-2 mm	4.2			618.8	1092	325	180	57	4.1
R ₁₋₂ C4	1-2 mm	5.6			582.4	1092	325	180	61	4.5
S ₅ R ₁₋₂ C1	1-2 mm		1.4		728.0	1092	325	180	60	2.3
S ₅ R ₁₋₂ C2	1-2 mm		2.8		692.6	1092	325	180	53	2.4
S ₅ R ₁₋₂ C3	1-2 mm		4.2		655.2	1092	325	180	54	3.0
S ₅ R ₁₋₂ C4	1-2 mm		5.6		618.8	1092	325	180	65	3.0
S ₁₀ R ₁₋₂ C1	1-2 mm			1.4	728	1092	325	180	63	2.4
S ₁₀ R ₁₋₂ C2	1-2 mm			2.8	692.6	1092	325	180	52	2.5
S ₁₀ R ₁₋₂ C3	1-2 mm			4.2	655.2	1092	325	180	55	3.0
S ₁₀ R ₁₋₂ C4	1-2 mm			5.6	618.8	1092	325	180	60	3.8
R ₂₋₄ C1	2-4 mm	1.4			728.0	1092	325	180	62	2.6
R ₂₋₄ C2	2-4 mm	2.8			692.6	1092	325	180	53	3.0
R ₂₋₄ C3	2-4 mm	4.2			655.2	1092	325	180	57	3.4
R ₂₋₄ C4	2-4 mm	5.6			618.8	1092	325	180	63	4.4
S ₅ R ₂₋₄ C1	2-4 mm		1.4		728.0	1092	325	180	63	2.3
S ₅ R ₂₋₄ C2	2-4 mm		2.8		692.6	1092	325	180	52	2.5
S ₅ R ₂₋₄ C3	2-4 mm		4.2		655.2	1092	325	180	60	2.5
S ₅ R ₂₋₄ C4	2-4 mm		5.6		618.8	1092	325	180	65	2.8
S ₁₀ R ₂₋₄ C1	2-4 mm			1.4	728.0	1092	325	180	60	2.5
S ₁₀ R ₂₋₄ C2	2-4 mm			2.8	692.6	1092	325	180	52	2.3
S ₁₀ R ₂₋₄ C3	2-4 mm			4.2	655.2	1092	325	180	59	2.7
S ₁₀ R ₂₋₄ C4	2-4 mm			5.2	618.8	1092	325	180	64	3.6

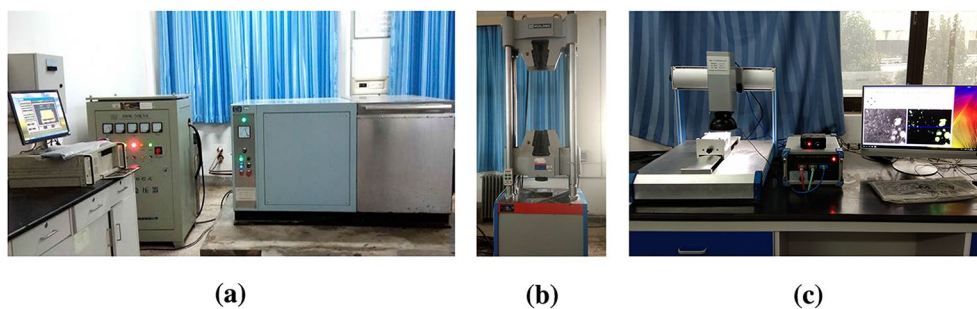


Fig. 2 The experimental setups of **a** CDR-5 automatic freeze–thaw test equipment, **b** WHY-2000 servo loading machine and **c** air-void analyzer

Table 3 The test design of freezing resistance

Freeze–thaw cycle	Measurement parameters	Test frequency	Termination of the test
GBT50082-2009 (2009); ASTM C666/C666M-15 (2015)	Mass loss rate: Eq. (1); Cube compressive strength (GB/T 50081–2019 (2019))	1/25	Mass loss rate ≥ 5.0%; Subjected to 100 cycles

Table 4 The measured W_n and F_n (%)

Specimens	W_0	W_{25}	W_{50}	W_{75}	W_{100}	F_0	F_{25}	F_{50}	F_{75}	F_{100}
C0	0.00	-0.14	0.19	0.69	2.56	100.00	97.51	92.89	86.02	76.63
R ₁₋₂ C1	0.00	-0.15	0.08	0.45	1.68	100.00	98.60	92.63	84.11	77.23
R ₁₋₂ C2	0.00	-0.30	-0.09	0.42	1.32	100.00	98.90	96.24	90.23	80.50
R ₁₋₂ C3	0.00	-0.43	-0.17	0.31	1.00	100.00	99.24	95.61	90.82	85.00
R ₁₋₂ C4	0.00	-0.56	-0.35	0.15	0.80	100.00	98.33	95.91	92.23	86.47
S ₅ R ₁₋₂ C1	0.00	-0.19	0.00	0.42	1.21	100.00	99.00	93.81	88.68	79.04
S ₅ R ₁₋₂ C2	0.00	-0.32	-0.13	0.28	0.93	100.00	99.31	95.04	91.29	81.52
S ₅ R ₁₋₂ C3	0.00	-0.50	-0.30	0.12	0.63	100.00	99.10	96.72	92.13	85.19
S ₅ R ₁₋₂ C4	0.00	-0.63	-0.45	-0.16	0.41	100.00	98.63	96.77	94.61	88.92
S ₁₀ R ₁₋₂ C1	0.00	-0.16	0.06	0.44	1.41	100.00	98.61	94.82	87.78	78.90
S ₁₀ R ₁₋₂ C2	0.00	-0.31	-0.05	0.35	1.09	100.00	98.60	95.44	89.40	81.52
S ₁₀ R ₁₋₂ C3	0.00	-0.46	-0.22	0.20	0.75	100.00	98.8	96.52	91.30	83.00
S ₁₀ R ₁₋₂ C4	0.00	-0.58	-0.40	-0.03	0.53	100.00	99.08	96.03	91.10	87.64
R ₂₋₄ C1	0.00	-0.14	0.13	0.53	1.79	100.00	98.40	94.22	87.04	77.03
R ₂₋₄ C2	0.00	-0.29	0.00	0.42	1.50	100.00	98.55	95.90	90.24	79.12
R ₂₋₄ C3	0.00	-0.42	-0.11	0.32	1.23	100.00	99.00	95.91	91.04	81.36
R ₂₋₄ C4	0.00	-0.55	-0.29	0.27	0.92	100.00	98.80	97.70	92.32	84.54
S ₅ R ₂₋₄ C1	0.00	-0.18	0.06	0.47	1.35	100.00	98.03	93.44	85.53	78.07
S ₅ R ₂₋₄ C2	0.00	-0.30	-0.08	0.34	1.01	100.00	98.80	96.33	90.26	80.50
S ₅ R ₂₋₄ C3	0.00	-0.44	-0.22	0.26	0.52	100.00	98.71	94.74	90.45	82.43
S ₅ R ₂₋₄ C4	0.00	-0.59	-0.38	0.00	0.43	100.00	98.30	96.60	93.43	86.47
S ₁₀ R ₂₋₄ C1	0.00	-0.16	0.09	0.52	1.58	100.00	97.77	93.28	86.26	76.54
S ₁₀ R ₂₋₄ C2	0.00	-0.30	-0.03	0.38	1.20	100.00	98.50	94.43	87.51	77.39
S ₁₀ R ₂₋₄ C3	0.00	-0.44	-0.19	0.29	0.94	100.00	99.10	96.34	90.44	81.21
S ₁₀ R ₂₋₄ C4	0.00	-0.57	-0.34	0.07	0.63	100.00	98.51	95.43	91.00	84.60

subscripts 0 and n ($0 \leq n \leq 100$) are used to express the freeze–thaw cycles.

3 Results and Discussion

3.1 Slump and Air Content of Fresh Concrete

The measured slumps obtained in this experiment are listed in Table 2. Little differences were observed between the slumps for the concrete with the pretreated rubber particles and that of the concrete with untreated particles. With increasing rubber content, concrete slumps first decreased and then increased slightly, reaching a minimum with a reduction of approximately 10.0% when the rubber content reached 2.8%, and this was similar to the author's previous study (Chen et al., 2021). The fresh concrete with rubber particles 2.00–4.00 mm in size exhibits a larger slump than that with particles 1.00–2.00 mm in size. This is to be expected since the decrease in the specific surface area of the rubber particle with increasing rubber size reduced the water absorption of the rubber aggregate.

As shown in Table 2, which lists measured air content of fresh concrete, the effects of rubber content, particle size, and pretreatment on air content were significant.

The air content increased significantly with an increase in rubber content, while there was a significant decrease obtained by pretreating the rubber. The hydrophobicity, roughness and porosity of the rubber interface enhanced the rubber's ability to carry air (Chen et al., 2020; Eiras et al., 2014); hence, the air content increased with increasing rubber content. The contact angle between the rubber and water was decreased by pretreating the rubber particle (Chou et al., 2007), indicating an increase in superficial hydrophilicity and a decrease in the air content. In addition, the decrease in the specific surface area of the rubber particles with increasing rubber size also weakened the rubber's ability to carry air.

3.2 Properties of Rubberized Concrete During Freeze–Thaw Cycles

3.2.1 Mass Loss Rate

Any loss of the saturated concrete weight during freeze–thaw cycles is the spalling of the concrete matrix caused by concrete damage, an important parameter for frost resistance of concrete. The measured mass loss rate (W_n) values of concrete after 0, 25, 50, 75 and 100 freeze–thaw cycles are listed in Table 4.

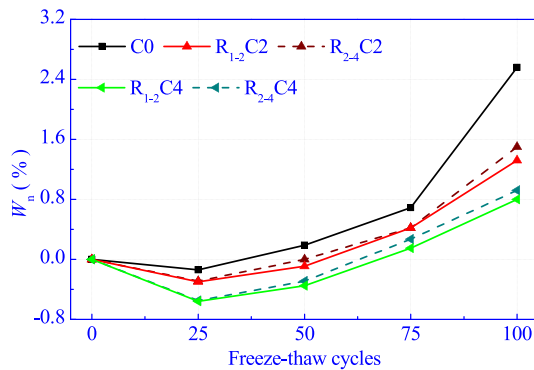
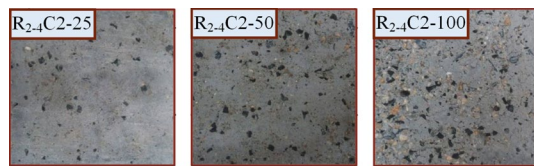


Fig. 3 The effects of rubber content on W_n

As shown in Fig. 3, there was a significant increase in W_n as more particles peeled off from the concrete matrix with the increase in freeze–thaw cycles, indicating worsening freeze–thaw damage. The W_n of rubberized concrete in the same freeze–thaw cycles decreased significantly with increasing rubber content, and the W_{100} of concrete with rubber particles of 1.00–2.00 mm in size was decreased from 2.6 to 0.8% by increasing the rubber content from 0.0 to 5.6%. The addition of rubber particles intensified the increase in concrete mass in early freeze–thaw cycles, and the W_n values of the rubberized concrete with rubber contents of 1.4–5.6% were negative, as shown in Fig. 3.

The average values for measured W_n for the rubberized concretes with rubber particles of 1.4%, 2.8%, 4.2% and 5.6% were used to analyze the effects of rubber particle size and the pretreatment on concrete W_n , which was represented by w_n . As shown in Fig. 4, rubberized concrete with rubber particles of smaller size exhibited a smaller w_n , and the surface freezing damage of $R_{2.4}C_4$ was more serious than that of $R_{1.2}C_4$ after 100 freeze–thaw cycles. In addition, the pretreatment of rubber particles significantly reduced concrete w_n , and sodium hydroxide solutions with mass concentrations of 5.0% exhibited a better pretreatment effect. The w_{100} of rubberized concrete with rubber particles of 1.00–2.00 mm in size decreased 33.3% when the rubber particles were pretreated with sodium hydroxide solutions with mass concentrations of 5.0%, and the surface freezing damage of $S_5R_{1.2}C_4$ was much less severe than that of $R_{1.2}C_4$ after 100 freeze–thaw cycles, as shown in Fig. 4.

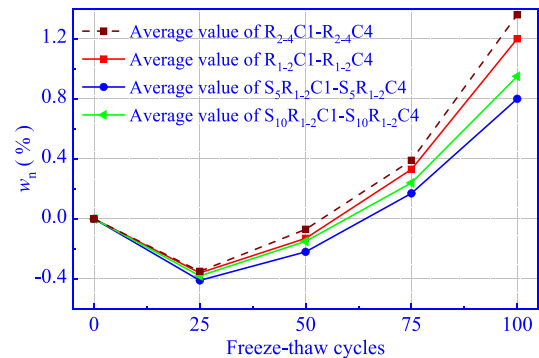


Fig. 4 The effects of rubber particle size and pretreatment on w_n

Similar to air-entraining agents, rubber aggregates improved concrete meso-void structures that resist damage during freeze–thaw cycles (Gonen, 2018; Medine et al., 2018). In this experiment, the air content of the fresh concrete with 5.6% rubber content reached 4.0%. During initial damage, concrete microcracks opened channels to internal voids, and the concrete mass increased via water absorption. The rubberized concrete with a larger porosity exhibited stronger water absorption; hence, the increase in mass for concrete with more rubber particles was larger. The smaller rubber particle has a larger specific surface area and improves the concrete meso-void structure more significantly than larger size particles. The enhanced superficial adsorption, roughness, and attenuation of the hydrophobicity of the rubber by rubber pretreatment helped reduce internal defects of rubberized concrete (Guo et al., 2017; Si et al., 2017) and inhibited destruction of the concrete matrix. Therefore, W_n decreased with increasing rubber content, and the addition of pretreated rubber particles of smaller size can further inhibit concrete freeze–thaw damage.

3.2.2 Compressive Strength

The concrete strength decreased significantly with increasing rubber content and increased to a fixed extent by rubber pretreatment, a result similar to existing studies (Gregori et al., 2019; Li et al., 2019; Siddika et al., 2019); this has been reported in parallel papers for the mechanical properties and dynamic properties of rubberized concrete (Chen et al., 2020, 2021). In this section, the change law of compressive strength for rubberized concrete in freeze–thaw cycles was studied

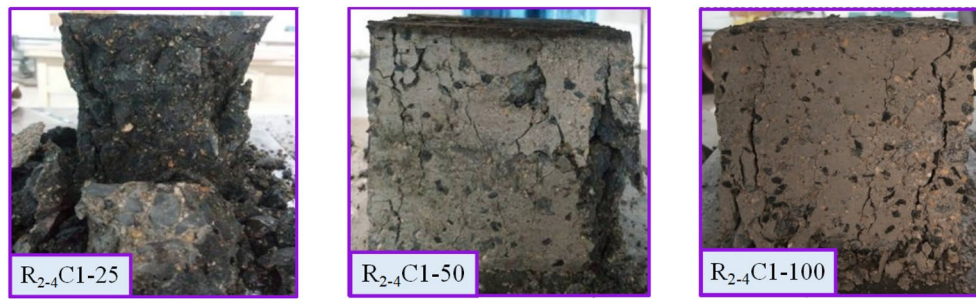


Fig. 5 The compressive failure patterns of $R_{2.4}C_4$ after 25, 50 and 100 freeze–thaw cycles

by analyzing the freeze–thaw test results of relative compressive strength (F_n). The measured F_n of concrete after 0, 25, 50, 75 and 100 freeze–thaw cycles is listed in Table 4.

As shown by the compressive failure patterns of $R_{2.4}C_4$ after 25, 50 and 100 freeze–thaw cycles in Fig. 5, the axial deformation and relative slippage of the concrete matrix increased, and the Poisson effect became more significant with increase in number of freeze–thaw cycles, showing a false appearance of deformation adaptability for concrete (Liu & Wang, 2012). However, this was in reality the macro-scale reflection of the freeze–thaw damage aggravating the concrete compressive damage (Berto et al., 2015). The evolution of compressive strength of rubberized concrete with different content of rubber particles with increase in number of freeze–thaw cycles was shown in (Fig. 6a). The F_n of concrete in the same freeze–thaw cycles increased significantly with an increase in rubber content, and the F_{100} of concrete with rubber particles of 1.00–2.00 mm in size increased from 76.6 to 86.5% when the rubber content increased from 0.0 to 5.6%, suggesting an optimum rubber content of 5.0–6.0% for maximum freeze–thaw protection (Chen et al., 2015; Richardson et al., 2012). This result indicated that efficient use of waste tire rubber in concrete as a material to enhance concrete frost resistance was feasible.

The effects of rubber particle size and the pretreatment on concrete F_n were studied by analyzing the average values of measured F_n , which was represented by f_n , for the rubberized concretes with rubber particles of 1.4%, 2.8%, 4.2% and 5.6%. As shown in Fig. 6, the f_n of rubberized concrete with 1.00–2.00 mm rubber particles in the same rubber content and freeze–thaw cycles were slightly larger than that of rubberized concrete with 2.00–4.00 mm rubber particles. The pretreatment of rubber particles increased f_n , and the sodium hydroxide solutions with mass concentrations of 5.0% exhibited a better pretreatment effect. This result and the changes law of w_n mentioned above indicated that utilizations of rubber particles with smaller sizes and effective pretreatment enhanced the frost resistance of rubberized concrete. However, the increase in f_n was limited by limits in decreasing rubber particle size and rubber pretreatment since the difference in the size between these two types of rubber particles was small. In addition, the effect of rubber pretreatment on concrete air content was much weaker than that on rubber content, as reported in Sect. 3.1.

The specific surface area of the rubber increased with decreasing rubber size and enhanced the rubber’s ability to carry air. The increase in the air bubbles with sizes of less than 350 μm (Wang et al., 2019) had a significant

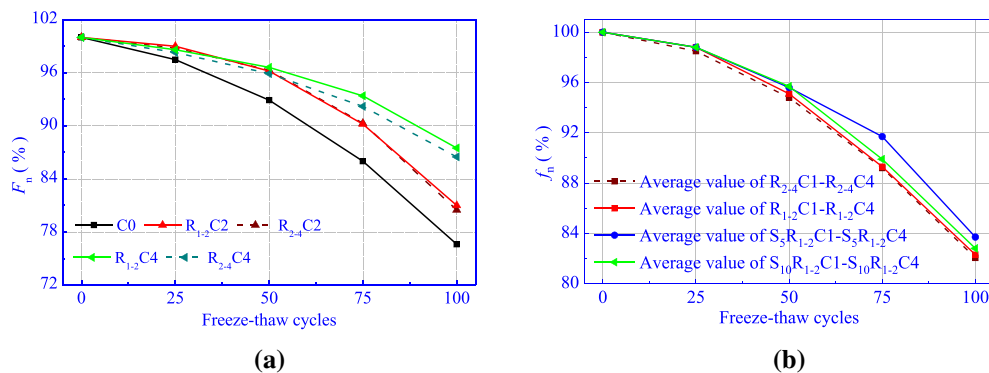


Fig. 6 Effects of **a** rubber content, size and **b** pretreatment on the changes of rubberized concrete F_n and f_n

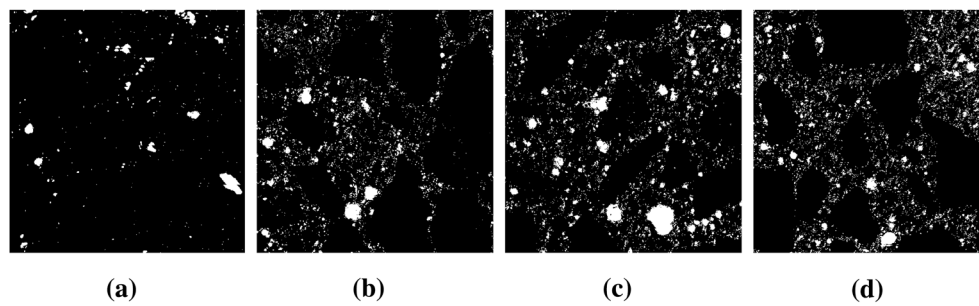


Fig. 7 The mesoscopic pore structure of rubberized concrete in the section of $30 \times 30 \text{ mm}^2$: **a** C0, **b** $R_{1-2}C_2$, **c** $R_{1-2}C_4$ and **d** $S_5R_{1-2}C_4$

effect on terminating the extension of frost heave microcracks and provided release space for the expansion and migration of ice and liquid water in concrete. The rubber pretreatment strengthened the bonding between rubber and the cement matrix (Guo et al., 2017; Si et al., 2017) and effectively reduced the number of harmful voids and cracks (Chen et al., 2021; Yuan et al., 2018). All of the abovementioned factors were beneficial for improving the frost resistance of rubberized concrete to a certain extent. Therefore, the auxiliary means to further improve rubberized concrete frost resistance can be performed by an appropriate design of rubber particle size and rubber pretreatment.

3.2.3 Mesostructure of Rubberized Concrete

The stable bubbles of appropriate size ($\leq 350 \mu\text{m}$) and spacing ($\geq 250 \mu\text{m}$) effectively shorten the distance from the concrete capillary pore water to the free surface and provide release spaces for the pore hydrostatic pressure, osmotic pressure, ice expansion pressure, etc., generated during the freeze–thaw process, thus enhancing the frost resistance of the concrete matrix (Powers, 1945; Richardson et al., 2016; Yuan et al., 2018). Therefore, studies on the mesostructural properties of rubberized concrete that analyze the influence of rubber particles on concrete frost resistance are important and necessary.

The air bubbles distributed in the $30 \times 30 \text{ mm}^2$ sample for C0, $R_{1-2}C_2$, $R_{1-2}C_4$ and $S_5R_{1-2}C_4$ are shown in (Fig. 7a, b, c and d). Both the number and volume of bubbles increased significantly with increasing rubber content, and the rubber pretreatment decreased the size of bubbles. In addition, the average bubble size of $R_{1-2}C_2$ was smaller than that of C0. The change in concrete air content with rubber content and the effect of rubber pretreatment on concrete air content are shown in Fig. 8 and are consistent with the phenomena above. With increasing rubber content, the air content of hardened concrete (A_h) increased significantly. The value of A_h increased to 11.4% for concrete with 20.0% rubber content, and it decreased to 10.2% by pretreating the rubber particles.

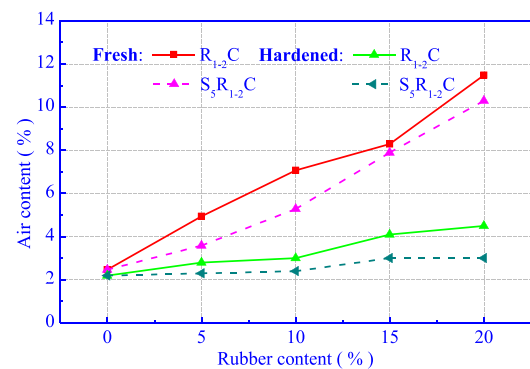


Fig. 8 Effects of rubber content and pretreatment on concrete air content

Different from the linear relationship between the air content of fresh concrete (A_f) and A_h for normal concrete (He et al., 2021; Pham et al., 2018), the value of A_h increased faster than that of A_f with the increase in rubber content since a portion of water absorbed by the rubber particle was consumed to form air bubbles.

Changes in the air content, W_{100} and F_{100} for the rubberized concrete are shown in Fig. 9. Similar to Pham et al. (2019) and Grinys et al. (2020), the frost resistance was enhanced significantly, with an obvious increase in F_{100} and $(1-W_{100})$, when samples contain pretreated rubber particles, but the concrete air content decreased. This can be attributed to the properties of the bubbles, such as the size, spacing, surface-volume ratio, etc. The measured average chord length (l), bubble diameter (d) and spacing coefficient (L) are shown in (Fig. 10a). The values of l and d first decreased with increasing rubber content and then increased consistently when the rubber content exceeded 15.0%. The values of l and d reduced significantly by rubber pretreatment. This result indicated the advantages of using rubber particles to improve concrete mesostructure and enhance the frost resistance. However, it is not the case that concrete with a larger air content exhibits better frost resistance. An excessively large air content decreased the bubble spacing, and microbubbles merged

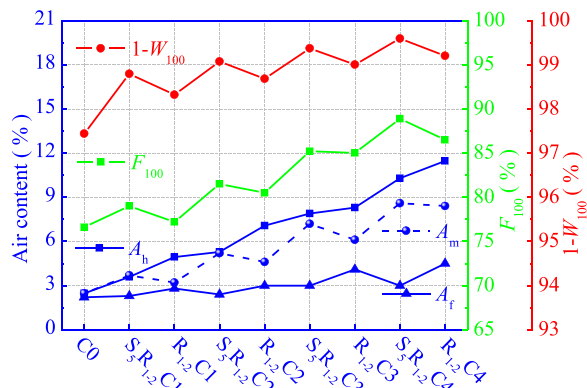


Fig. 9 Changes of the air content, W_r , and F_n for the rubberized concrete

into larger bubbles, and this was detrimental to the concrete frost resistance. As shown in Fig. 10, the value of L decreased notably with increasing rubber content, and the bubble surface–volume ratio decreased when the rubber content exceeded 15.0%.

In addition to the effects of bubble properties, the weak rubber–cement matrix interface, microcracks, and other adhesion defects caused by adding rubber particles reduced the frost resistance of rubberized concrete. It has been proven in a parallel study paper (Chen et al., 2021) analyzing the mesostructure of rubberized concrete with scanning electron microscopy that the rubber–cement matrix interface was strengthened and the adhesion defects were reduced significantly by pretreating rubber particles. This was another important reason for the better frost resistance of the pretreated rubberized concrete compared to the concrete with untreated rubber particles in the same content. Therefore, neither the change in A_f nor

A_h was consistent with that of concrete frost resistance, as shown in Fig. 9. The A_h of rubberized concrete consists of A_f and voids formed during the hydration of concrete. Most of these voids were formed by the consumption of the water absorbed by the rubber particles, the weak rubber–cement matrix interface, microcracks, and other adhesion defects due to the hydrophobicity of rubber.

Based on the studies above, to quantify the effects of rubber content and pretreatment on concrete frost resistance, two assumptions were made: (1) the air content of hardened concrete mixed with rubbers of the same content and particle size is determined by the surface characteristics of the rubber particles. (2) Only the voids harmful to the frost resistance of rubberized concrete are reduced by pretreating rubber particles. Based on these assumptions, the relationship between effective air content (A_m) of hardened rubberized concrete to its frost resistance was determined by Eq. (3):

$$A_m = A_f + \alpha \rho_r - \Delta A_h, \tag{3}$$

where α and ρ_r are the coefficient and rubber content, respectively, and α is related to the size of the rubber particles. ΔA_h is the reduced content of the voids that are harmful to rubberized concrete frost resistance and is approximately by $(A_{fp} - A_{fu})$ where A_{fp} and A_{fu} are the air content of pretreated rubberized concrete and the concrete with untreated rubber particles, respectively. As shown in Fig. 9, the change in A_m is consistent with that of concrete frost resistance. In addition, it has been proven through many analyses and experimental studies (Han, 2022) that Eq. (3) is also applicable to rubberized concrete with rubber powders of smaller size. Therefore, it is satisfactory to quantify effects of rubber particles on compressive strength during freeze–thaw cycles using A_m .

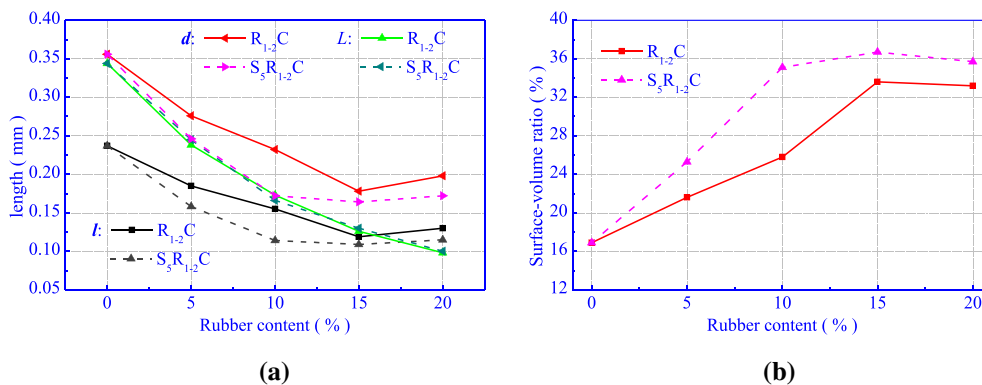


Fig. 10 Properties of concrete bubbles: **a** measured bubble average chord length (l), diameter (d), spacing (L); and **b** surface–volume ratio

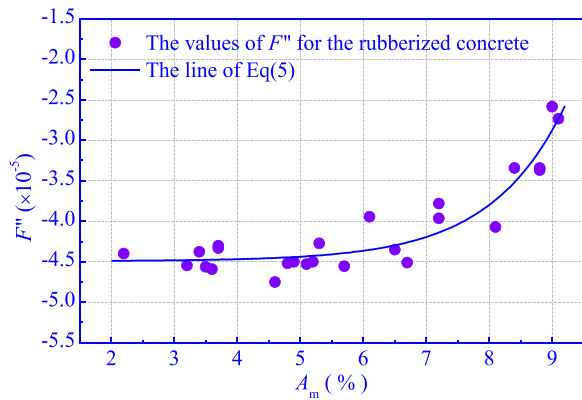


Fig. 11 Relationship of $(\partial^2 F / \partial n^2)$ and A_m

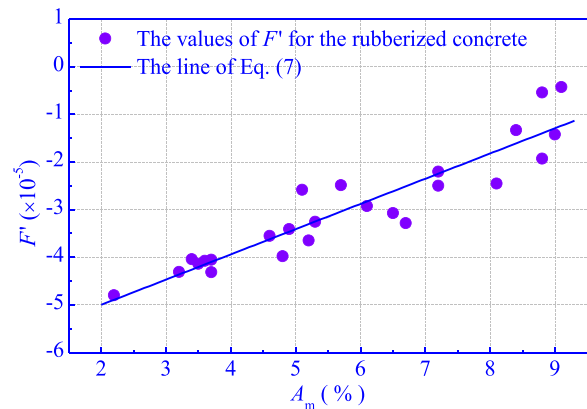


Fig. 12 Relationship of $(\partial F / \partial n)$ and A_m

4 Evaluation of Compressive Strength During Freeze–Thaw Cycles

4.1 Establishment of the Forecast Model

At present, freeze–thaw damage models of normal concrete have been proposed by researchers in different functional forms, such as exponential functions, power functions and other complex functions (Chen & Qiao, 2015; Long et al., 2019; Wang et al., 2020). On this basis, a function related to the concrete mesostructure and freeze–thaw cycles (n) was appropriate for expressing the change in compressive strength for the rubberized concrete:

$$F_n = F(n, A_m). \tag{4}$$

According to the test results shown in Fig. 5 and Fig. 6, Eq. (4) was satisfactory as a function of quadratic polynomial for each group of concrete with the known value of A_m , and $(\partial^2 F / \partial n^2)$ was a value determined from test results by least square fitting. The effect of rubber particles on the change in concrete compressive strength during freeze–thaw cycles can be expressed quantitatively by establishing the quantitative relationship between $(\partial^2 F / \partial n^2)$ and A_m . Then, the forecast model for rubberized concrete compressive strength in freeze–thaw cycles can be determined.

To clarify the relationship $(\partial^2 F / \partial n^2)$ expressed as F'' with A_m for the concrete in this test, the values of F'' and A_m are plotted in Fig. 11 by assigning F'' to the x-axis and A_m to the y-axis. The ranges of the rubberized concrete f_{cu} , rubber size and content were 22.10–37.80 MPa, 1.00–4.00 mm, and 0.0–20.0% (0.0–5.6% by the concrete volume), respectively. In addition, the effects of the pretreatment of rubber particles were also considered. As shown in Fig. 11, the data were distributed along the curve of an exponential function which was expressed as Eq. (5) with an R-squared of 0.8743:

$$F'' = -4.4926 + 0.0008e^{0.8458A_m}. \tag{5}$$

Based on Eq. (5), $(\partial F / \partial n)$, which is expressed as F' , can be determined by Eq. (6):

$$F' = (-4.4926 + 0.0008e^{0.8458A_m})n + \varphi(A_m), \tag{6}$$

where $\varphi(A_m)$ is related to the mesostructure of rubberized concrete, as expressed by Eq. (7):

$$\varphi(A_m) = \lim_{\Delta x \rightarrow 0} \frac{F(0 + \Delta x) - F(\Delta x)}{\Delta x}. \tag{7}$$

On this basis, the relationship between $\varphi(A_m)$ and A_m can be clarified, as shown in Fig. 12. $\varphi(A_m)$ and A_m are linearly correlated, and $\varphi(A_m)$ was expressed by Eq. (8) with an R-squared value of 0.8623:

$$\varphi(A_m) = -6.0584 + 5.2963A_m. \tag{8}$$

Using boundary conditions of $n=0$ for the rubberized concrete, the value of F_0 was calculated to be 1.0000. The forecast model for compressive strength for rubberized concrete in freeze–thaw cycles can be expressed as Eq. (9):

$$F_n = an^2 + bn + 1.0000, \tag{9}$$

where a and b are the parameters obtained from Eq. (10) and Eq. (11), respectively, and are based on Eqs. (3)–(8):

$$a = (-2.2463 + 0.0008e^{0.8458A_m}) \times 10^{-5}, \tag{10}$$

$$b = (-6.0584 + 5.2963A_m) \times 10^{-5}. \tag{11}$$

The comparison of the test values of all the concrete samples in this experiment and the predicted curve of Eq. (9) are shown in Fig. 13. Yuan et al. (2018) and Yang et al.

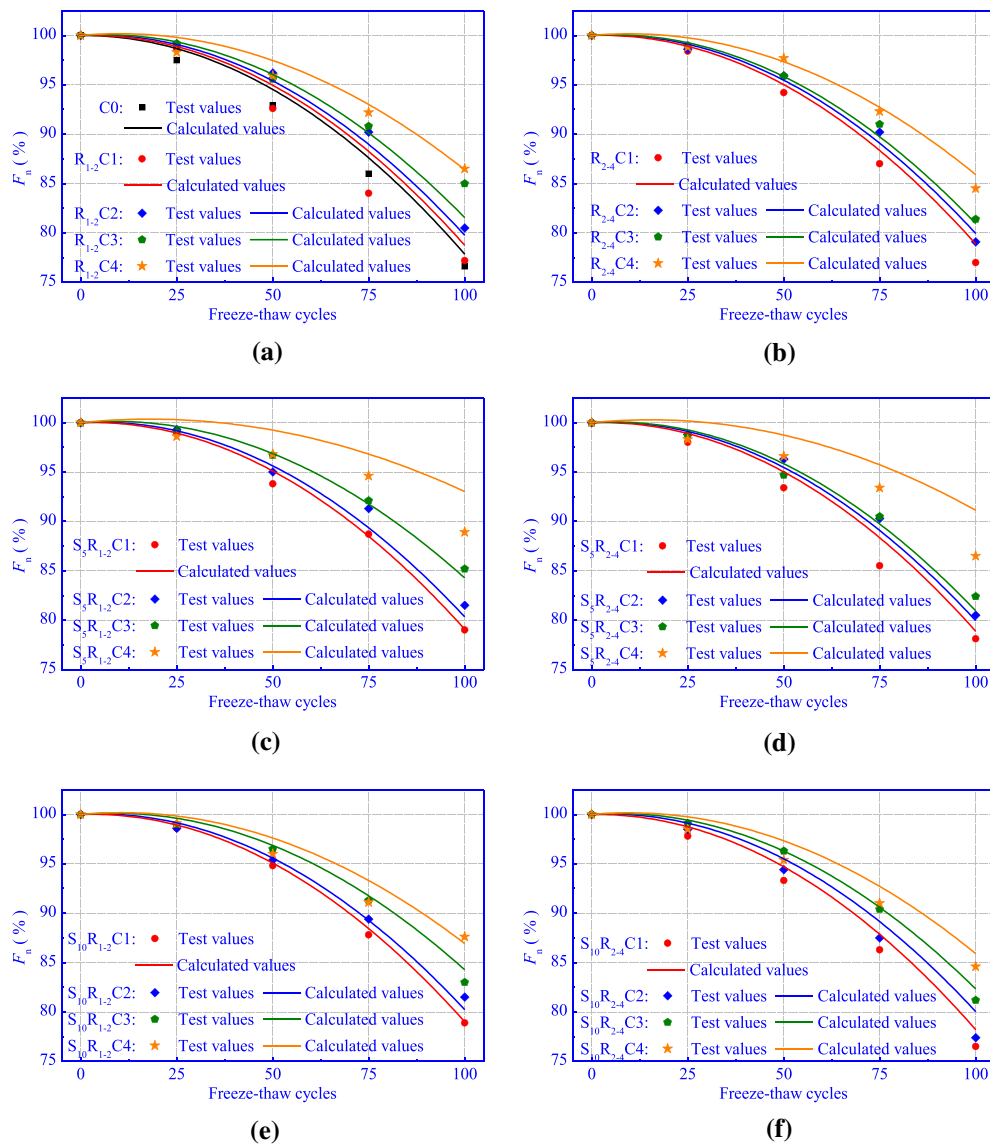


Fig. 13 The comparison of the predicted curves and test values of all the concrete: (a, b) rubberized concrete with untreated rubber particles in size of 1-2 mm and 2-4 mm, respectively, (c, d) rubberized concrete with rubber particles in size of 1-2 mm and 2-4 mm pretreated by sodium hydroxide solution with mass concentrations of 5.0%, and (e, f) rubberized concrete with rubber particles in size of 1-2 mm and 2-4 mm pretreated by sodium hydroxide solution with mass concentrations of 10.0%

(2008) reported that the spacing of the bubbles decreased, and the bubbles merged into larger bubbles significantly when the air content exceeded 8.3%, and this was unfavorable to the frost resistance of concrete. In this study, a similar result was obtained: the theoretical frost resistance of the rubberized concrete with an A_m of more than 8.0% was much larger than the test results, as shown by the comparison of the test values and the predicted curves for $S_5R_{1.2}C_4$ and $S_5R_{2.4}C_4$ shown in Fig. 13 (a) and (b). Comparing the calculated values to the test values, the maximum relative error was 5.3%, and the goodness of fit was 0.9844,

indicating a satisfactory fit between the forecast model and the experimental values.

4.2 Application of the Forecast Model

Based on Eq. (9), the compressive strength of the rubberized concrete in no more than 100 freeze–thaw cycles can be calculated. To verify the accuracy and application of the forecast model, a total of 190 groups of data containing 125 of the authors’ groups and 65 groups from other scholars (Han, 2022; Richardson et al., 2012; Wang & Su, 2016; Wang et al., 2020; Xu et al., 2012) were

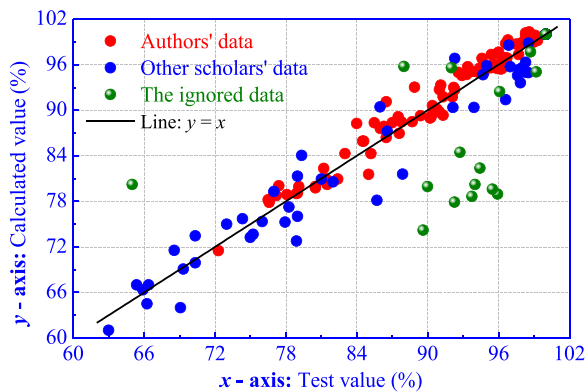


Fig. 14 Comparison of tested values and calculated values with Eq. (9)

collected. Comparing the values calculated by Eq. (9) to the test values and ignoring the five groups with abnormally large relative errors of 23.4% and 39.1% in reference (Wang & Su, 2016), 17.1% in reference (Wang et al., 2020), and 19.4% and 63.3% in reference (Han, 2022), the maximum and mean relative errors were 15.6% and 2.7%, respectively. The goodness of fit was 0.9519, indicating a satisfactory fit between the forecast model and the test values.

The ranges of the water–cement ratio, compressive strength, rubber size and content for the concrete mentioned above were 0.44–0.72, 19.10–64.90 MPa, 0.15–4.00 mm, and 0.0–20.0%, respectively. In addition, it contained multiple pretreatment methods, such as rubber pretreatment with 5.0% sodium hydroxide solution, 10.0% sodium hydroxide solution, silane coupling agent, etc. Among these, the five ignored groups of concrete with abnormally large relative errors were analyzed deeply. The difference in the calculated values and the test values for the five groups of concrete mentioned above were especially larger than that of the other data due to their extremely low strength and the poor meso-void structure resulting from the addition of a large amount of recycled aggregates and rubber particles. The water–cement ratio of the concrete ignored in reference (Wang & Su, 2016) was 0.72. The values of A_m for the concrete ignored in references (Han, 2022; Wang et al., 2020) all exceeded 8.0%, and they reached 10.8% for the concrete with 4.0% rubber powder with a size of 0.15 mm.

All data are plotted in Fig. 14. The calculated values of F_n for concretes within 100 freeze–thaw cycles were obtained by Eq. (9), and the comparisons to the test values are also shown in Fig. 14, which plots the experimental values on the x-axis and the calculated values on the y-axis. With the exception of the five groups of concrete with abnormally large relative errors, the data were

distributed along a line. Therefore, the forecast model exhibited satisfactory accuracy and has good application potential toward evaluating the compressive strength of rubberized concrete. It should be noted that the ranges of water–cement ratio must be 0.44–0.60, the compressive strength should be no more than 60.00 MPa; rubber particle size should be 0.15–4.00 mm; content for the rubberized concrete should be 0.0–20.0%, and the value of A_m should be no more than 8.0%.

The forecast model of compressive strength for rubberized concrete with a good predictive ability has been proposed in a parallel study paper (Chen et al., 2022) about analytical evaluation of compressive strength for concrete with rubber fine aggregates. On the basis, the initial cube compressive strength of rubberized concrete can be expressed as Eq. (12). Finally, the compressive strength of rubberized concrete in freeze–thaw cycles can be calculated with Eq. (13) based on the quantitative relationship among $f_{cu,0}$, $f_{cu,n}$ and F_n (Eq. (2), Eq. (9) and Eq. (12)), and the effects of rubber particle size, content and the pretreatment are considered:

$$f_{cu,0} = 10.8425f_b \left(1 + \rho_b \frac{m_w / \rho_w + A_m}{m_b}\right)^{-2.4324}, \quad (12)$$

$$f_{cu,n} = 10.8425f_b (an^2 + bn + 1.0000) \left(1 + \rho_b \frac{m_w / \rho_w + A_m}{m_b}\right)^{-2.4324}, \quad (13)$$

where f_b is the compressive strength of the cementitious material at 28 days, and m_b and ρ_b are the mass and density of the cementitious material, respectively. Besides, m_w and ρ_w represent the mass and density of the water, respectively.

The forecast model proposed in this study was satisfactory to calculate the compressive strength of rubberized concrete of 20.00–50.00 MPa with the water–cement ratio of 0.44–0.60 within 100 freeze–thaw cycles. In addition, the rubber particles were untreated and pretreated in size of no larger than 4.00 mm, including the single particle size and continuous grading. Considering the significant effects of concrete void structure on the frost resistance, the rubber content and A_m shall not exceed 4.2% and 8.0%. The forecast model exhibited feasible predictive ability for the rubberized concrete mentioned above within 100 freeze–thaw cycles. In view of the rapid deterioration of concrete strength in the later stage of freeze–thaw failure, further study on rubberized concrete compressive strength more than 100 freeze–thaw cycles and the modification of the forecast model to feasibly evaluate the change law of compressive strength

for the rubberized concrete in freeze–thaw cycles will be conducted.

5 Conclusions

In this paper, the change in compressive strength of rubberized concrete with rubber fine aggregates of different sizes, contents and pretreatments during freeze–thaw cycles was studied from the macro- and meso-perspectives, and the following conclusions can be drawn:

- (1) The decrease in concrete strength and weight was notably restricted by the presence of rubber particles during freeze–thaw cycles. The pretreated rubber particles with smaller particle sizes enhanced the concrete frost resistance more significantly. The F_{100} of concrete with rubber particles of 1.00–2.00 mm increased from 76.6% to 86.5% by increasing the rubber content from 0.0% to 5.6%.
- (2) The influence of rubber fine aggregates on concrete frost resistance was examined, and the effects of rubber fine aggregates on concrete frost resistance can be quantified with the change in the concrete mesostructure. It is satisfactory to quantize the effects of rubber particles on compressive strength during freeze–thaw cycles by using A_m .
- (3) A forecast model was proposed to calculate the compressive strength of rubberized concrete during freeze–thaw cycles. In the model, the effects of rubber particle size, content, and pretreatment are considered. The calculation results agree well with the experimental results when compared with peer studies, and this indicates that the proposed formulas can provide a good reference for the design and application of rubberized concrete in frigid environments.

Acknowledgements

The authors would like to acknowledge the editors and reviewers, and their selfless work and valuable comments that made a substantial improvement to this manuscript.

Author contributions

SS and XH performed the experimental works, analyzed data and wrote the manuscript. AC and QZ reviewed and commented the manuscript regarding the freeze–thaw cycle test of rubberized concrete. ZW and KL reviewed and commented the experimental design, properties of the fresh and hardened rubberized concrete. All authors read and approved the final manuscript.

Author information

SS, M.Eng., School of Civil Engineering and Communication. XH, Ph.D. Lecturer, School of Civil Engineering and Communication. AC, Ph.D. Professor, Doctoral advisor, School of Water Conservancy. QZ, Ph.D. Professor, Doctoral advisor, State Key Lab Hydrol Water Resources & Hydraul En; Dept Engr Mech. ZW, Ph.D. Professor, Doctoral advisor, School of Civil Engineering and Communication. KL, Ph.D. Professor, School of Civil Engineering and Communication.

Funding

This work was supported by the National Natural Science Foundation of China (52179133, 11932006).

Availability of data and materials

The datasets used and analyzed during the current study are available from the corresponding author on reasonable request.

Declarations

Competing interests

The authors declare that they have no competing interests.

Received: 4 November 2022 Accepted: 14 February 2023

Published online: 09 May 2023

References

- Assaggaf, R., Maslehuddin, M., Al-Osta, M. A., Al-Dulajjan, S. U., & Ahmad, S. (2022). Properties and sustainability of treated crumb rubber concrete. *Journal of Building Engineering*. <https://doi.org/10.1016/j.jobbe.2022.104250>
- Berto, L., Saetta, A., & Talledo, D. (2015). Constitutive model of concrete damaged by freeze–thaw action for evaluation of structural performance of RC elements. *Construction and Building Materials*, 98, 559–569. <https://doi.org/10.1016/j.conbuildmat.2015.08.035>
- Chen, A., Han, X., Chen, M., Wang, X., Wang, Z., & Guo, T. (2020). Mechanical and stress–strain behavior of basalt fiber reinforced rubberized recycled coarse aggregate concrete. *Construction and Building Materials*. <https://doi.org/10.1016/j.conbuildmat.2020.119888>
- Chen, A., Han, X., Wang, Z., & Guo, T. (2021). Dynamic properties of pretreated rubberized concrete under incremental loading. *Materials*. <https://doi.org/10.3390/ma14092183>
- Chen, A., Han, X., Wang, Z., Zhang, Q., Xia, X., Ji, Y., & Li, K. (2022). Analytical evaluation of compressive strength for concrete with rubber fine aggregates and the predictive model. *Construction and Building Materials*. <https://doi.org/10.1016/j.conbuildmat.2022.128359>
- Chen, A., Wang, J., & Ma, Y. (2015). Test of frost resistance for steel fiber rubber recycled concrete. *Acta Materiae Compositae Sinica*, 32(04), 933–941. <https://doi.org/10.13801/j.cnki.fhclxb.20141022.006>
- Chen, F., & Qiao, P. (2015). Probabilistic damage modeling and service-life prediction of concrete under freeze–thaw action. *Materials and Structures*, 48(8), 2697–2711. <https://doi.org/10.1617/s11527-014-0347-y>
- Chou, L. H., Lu, C. K., Chang, J. R., & Lee, M. T. (2007). Use of waste rubber as concrete additive. *Waste Management and Research*, 25(1), 68–76. <https://doi.org/10.1177/0734242x07067448>
- Dvorkin, L. (2019). Design estimation of concrete frost resistance. *Construction and Building Materials*, 211, 779–784. <https://doi.org/10.1016/j.conbuildmat.2019.03.108>
- Eiras, J. N., Segovia, F., Borrachero, M. V., Monzó, J., Bonilla, M., & Payá, J. (2014). Physical and mechanical properties of foamed Portland cement composite containing crumb rubber from worn tires. *Materials and Design*, 59, 550–557. <https://doi.org/10.1016/j.matdes.2014.03.021>
- Gesoglu, M., Güneysi, E., Khoshnaw, G., & Ipek, S. (2014). Investigating properties of pervious concretes containing waste tire rubbers. *Construction and Building Materials*, 63, 206–213. <https://doi.org/10.1016/j.conbuildmat.2014.04.046>
- Gonen, T. (2018). Freezing–thawing and impact resistance of concretes containing waste crumb rubbers. *Construction and Building Materials*, 177, 436–442. <https://doi.org/10.1016/j.conbuildmat.2018.05.105>
- Gong, S., Zhang, W., & Zhang, J. (2018). Frost resistance and impact properties of roller compacted concrete mixed with rubber particles and steel fibers. *Acta Materiae Compositae Sinica*, 35(08), 2199–2207. <https://doi.org/10.13801/j.cnki.fhclxb.20170920.002>
- Gregori, A., Castoro, C., Marano, G. C., & Greco, R. (2019). Strength reduction factor of concrete with recycled rubber aggregates from tires. *Journal of Materials in Civil Engineering*. [https://doi.org/10.1061/\(ASCE\)MT.1943-5533.0002783](https://doi.org/10.1061/(ASCE)MT.1943-5533.0002783)

- Grinys, A., Augonis, A., Daukšys, M., & Pupeikis, D. (2020). Mechanical properties and durability of rubberized and SBR latex modified rubberized concrete. *Construction and Building Materials*. <https://doi.org/10.1016/j.conbuildmat.2020.118584>
- Guo, S., Dai, Q., Si, R., Xiao, S., & Chao, L. (2017). Evaluation of properties and performance of rubber-modified concrete for recycling of waste scrap tire. *Journal of Cleaner Production*, 148, 681–689. <https://doi.org/10.1016/j.jclepro.2017.02.046>
- Han, X. (2020). Wasted tires turn into 'Black gold'. *China Tire Resources Recycling*, 08, 21–23. <https://doi.org/10.19307/j.cnki.ctr.2020.08.006>
- Han, X. (2022). Experimental study on the predictive model of hydraulic rubberized concrete mechanical properties and freeze-thaw damage. *North China University of Water Resources and Electric Power*. <https://doi.org/10.27144/d.cnki.ghbsc.2022.000003>
- He, L., Cai, H. D., Huang, Y., Ma, Y., Bergh, W., Gaspar, L., Valentin, J., Vasiliev, Y. E., Kowalski, K. J., & Zhang, J. H. (2021). Research on the properties of rubber concrete containing surface-modified rubber powders. *Journal of Building Engineering*. <https://doi.org/10.1016/j.jobe.2020.101991>
- He, L., Huang, Y., Feng, C., & Ma, Y. (2018). Research progress on properties of rubberized concrete and the surface modification of crumb rubber. *Bulletin of the Chinese Ceramic Society*, 37(8), 2483–2489. <https://doi.org/10.16552/j.cnki.issn1001-1625.2018.08.022>
- Hu, J., & Wu, J. (2019). Mechanical properties and uni-axial compression stress-strain relation of recycled coarse aggregate concrete subjected to salt-frost cycles. *Construction and Building Materials*, 197, 652–666. <https://doi.org/10.1016/j.conbuildmat.2018.11.213>
- Huda, S. B., & Alam, M. S. (2015). Mechanical and freeze-thaw durability properties of recycled aggregate concrete made with recycled coarse aggregate. *Journal of Materials in Civil Engineering*. [https://doi.org/10.1061/\(ASCE\)MT.1943-5533.0001237](https://doi.org/10.1061/(ASCE)MT.1943-5533.0001237)
- Jafari, K., & Toufigh, V. (2017). Experimental and analytical evaluation of rubberized polymer concrete. *Construction and Building Materials*, 155, 495–510. <https://doi.org/10.1016/j.conbuildmat.2017.08.097>
- Li, L., Tu, G., Lan, C., & Liu, F. (2016). Mechanical characterization of waste-rubber-modified recycled-aggregate concrete. *Journal of Cleaner Production*, 124, 325–338. <https://doi.org/10.1016/j.jclepro.2016.03.003>
- Li, Y., Zhang, X., Wang, R., & Lei, Y. (2019). Performance enhancement of rubberized concrete via surface modification of rubber: a review. *Construction and Building Materials*. <https://doi.org/10.1016/j.conbuildmat.2019.116691>
- Liu, M., & Wang, Y. (2012). Damage constitutive model of fly ash concrete under freeze-thaw cycles. *Journal of Materials in Civil Engineering*, 24(09), 1165–1174. [https://doi.org/10.1061/\(ASCE\)MT.1943-5533.0000491](https://doi.org/10.1061/(ASCE)MT.1943-5533.0000491)
- Long, G., Yang, Z., Bai, C., Ma, K., & Xie, Y. (2019). Durability and damage constitutive model of filling layer self-compacting concrete subjected to coupling action of freeze-thaw cycles and load. *Journal of the Chinese Ceramic Society*, 47(07), 855–864. <https://doi.org/10.14062/j.issn.0454-5648.2019.07.05>
- Medine, M., Trouzine, H., De Aguiar, J. B., & Asroun, A. (2018). Durability properties of five years aged lightweight concretes containing rubber aggregates. *Periodica Polytechnica Civil Engineering*, 62(02), 386–397. <https://doi.org/10.3311/PPci.11363>
- Pacheco-Torres, R., Cerro-Prada, E., Escolano, F., & Varela, F. (2018). Fatigue performance of waste rubber concrete for rigid road pavements. *Construction and Building Materials*, 176, 539–548. <https://doi.org/10.1016/j.conbuildmat.2018.05.030>
- Pelisser, F., Zavarise, N., Longo, T. A., & Bernardin, A. M. (2011). Concrete made with recycled tire rubber: Effect of alkaline activation and silica fume addition. *Journal of Cleaner Production*, 19(6–7), 757–763. <https://doi.org/10.1016/j.jclepro.2010.11.014>
- Pham, N. P., Toumi, A., & Turatsinze, A. (2018). Rubber aggregate-cement matrix bond enhancement: Microstructural analysis, effect on transfer properties and on mechanical behaviours of the composite. *Cement and Concrete Composites*, 94, 1–12. <https://doi.org/10.1016/j.cemconcomp.2018.08.005>
- Pham, N. P., Toumi, A., & Turatsinze, A. (2019). Effect of an enhanced rubber-cement matrix interface on freeze-thaw resistance of the cement-based composite. *Construction and Building Materials*, 207, 528–534. <https://doi.org/10.1016/j.conbuildmat.2019.02.147>
- Pilehvar, S., Szczotok, A. M., Rodríguez, J. F., Valentini, L., Lanzon, M., Pamies, R., & Kjoniksen, A. L. (2019). Effect of freeze-thaw cycles on the mechanical behavior of geopolymer concrete and Portland cement concrete containing micro-encapsulated phase change materials. *Construction and Building Materials*, 200, 94–103. <https://doi.org/10.1016/j.conbuildmat.2018.12.057>
- Powers, T. C. (1945). A working hypothesis for further studies of frost resistance of concrete. *Journal of the American Concrete Institute*, 16(4), 245–272.
- Rahman, M., Al-Ghalib, A., & Mohammad, F. (2013). Anti-vibration characteristics of rubberised reinforced concrete beams. *Materials and Structures*, 47(11), 1807–1815. <https://doi.org/10.1617/s11527-013-0151-0>
- Richardson, A. E., Coventry, K. A., Edmondson, V., & Dias, E. (2016). Crumb rubber used in concrete to provide freeze-thaw protection (optimal particle size). *Journal of Cleaner Production*, 112, 599–606. <https://doi.org/10.1016/j.jclepro.2015.08.028>
- Richardson, A. E., Coventry, K. A., & Ward, G. (2012). Freeze/thaw protection of concrete with optimum rubber crumb content. *Journal of Cleaner Production*, 23(1), 96–103. <https://doi.org/10.1016/j.jclepro.2011.10.013>
- Si, R., Guo, S., & Dai, Q. (2017). Durability performance of rubberized mortar and concrete with NaOH-Solution treated rubber particles. *Construction and Building Materials*, 153, 496–505. <https://doi.org/10.1016/j.conbuildmat.2017.07.085>
- Siddika, A., Al Mamun, M. A., Alyousef, R., Amran, Y. H. M., Aslani, F., & Alabduljabbar, H. (2019). Properties and utilizations of waste tire rubber in concrete: a review. *Construction and Building Materials*, 224, 711–731. <https://doi.org/10.1016/j.conbuildmat.2019.07.108>
- Torretta, V., Rada, E. C., Ragazzi, M., Trulli, E., Istrate, I. A., & Cioca, L. I. (2015). Treatment and disposal of tyres: Two EU approaches: a review. *Waste Management*, 45, 152–160. <https://doi.org/10.1016/j.wasman.2015.04.018>
- Wang, B., Wang, F., & Wang, Q. (2018a). Damage constitutive models of concrete under the coupling action of freeze-thaw cycles and load based on Lemaitre assumption. *Construction and Building Materials*, 173, 332–341. <https://doi.org/10.1016/j.conbuildmat.2018.04.054>
- Wang, C., Liu, L., Cao, F., & Lu, L. (2020). Experimental study on mechanical properties of recycled concrete after freeze-thaw cycles. *Journal of Building Structures*, 41(12), 193–202. <https://doi.org/10.14006/j.jzjgxb.2018.0542>
- Wang, D., Yuan, Q., Shi, C., Cao, H., Feng, L., & Ma, Y. (2018b). Application of modified rubber concrete in canal lining of Zhaokou irrigation region. *Yellow River*, 40(3), 123–125. <https://doi.org/10.3969/j.issn.1000-1379.2018.03.028>
- Wang, J., Dai, Q., Si, R., & Guo, S. (2019). Mechanical, durability, and microstructural properties of macro synthetic Polypropylene (PP) fiber-reinforced rubber concrete. *Journal of Cleaner Production*, 234, 1351–1366. <https://doi.org/10.1016/j.jclepro.2019.06.272>
- Wang, Z., & Su, H. (2016). Correlation between recycled rubber concrete strength and damage evolution in freeze thaw cycles. *Journal of the Chinese Ceramic Society*, 35(12), 4286–4291. <https://doi.org/10.16552/j.cnki.issn1001-1625.2016.12.066>
- Xie, J. H., Zheng, Y. W., Guo, Y. C., Ou, R. X., Xie, Z. H., & Huang, L. (2019). Effects of crumb rubber aggregate on the static and fatigue performance of reinforced concrete slabs. *Composite Structures*. <https://doi.org/10.1016/j.composites.2019.111371>
- Xu, B., Bompaa, D. V., & Elghazouli, A. Y. (2020). Cyclic stress-strain rate-dependent response of rubberised concrete. *Construction and Building Materials*. <https://doi.org/10.1016/j.conbuildmat.2020.119253>
- Xu, J., Feng, X., & Chen, S. (2012). Effects of rubber aggregate on the frost resistance of concrete. *Journal of Northeastern University*, 33(06), 895–898.
- Yang, Q., Zhang, S., Yang, Q., & Ji, W. (2008). Effects of air-entraining agent on air void parameters of concrete. *Journal of Tongji University*, 03, 374–378.
- Yu, Y., & Zhu, H. (2016). Influence of rubber size on properties of crumb rubber mortars. *Materials*. <https://doi.org/10.3390/ma9070527>
- Yuan, Q., Li, Y., Feng, X., et al. (2017). Study and application for the rubber concrete of high performance with high abrasion resistance, Zhengzhou, China. <https://kns.cnki.net/KCMS/detail/detail.aspx?dbname=SNAD&filename=SNAD000001681860>
- Yuan, J., Wu, Y., & Zhang, J. (2018). Characterization of air voids and frost resistance of concrete based on industrial computerized tomographical technology. *Construction and Building Materials*, 168, 975–983. <https://doi.org/10.1016/j.conbuildmat.2018.01.117>
- Zhang, Y., Zhao, Z., Chen, S., & Sun, W. (2006). Impact of rubber powder on frost resistance of concrete in water and NaCl solution. *Journal of Southeast University*, S2, 248–252.

- Zhao, Y., Fan, X., Wand, L., & Shi, J. (2017). Attenuation model of mechanical properties of concrete under different freezing and thawing. *Acta Materiae Compositae Sinica*, 34(02), 463–470. <https://doi.org/10.13801/j.cnki.fhclxb.20160425.001>
- Zhu, J., Li, S., Liu, X., & Liu, M. (2009). Mechanical property deterioration model for concrete in environment with freezing-thawing. *Journal of Architecture and Civil Engineering*, 26(01), 62–67.

Publisher's Note

Springer Nature remains neutral with regard to jurisdictional claims in published maps and institutional affiliations.

Submit your manuscript to a SpringerOpen[®] journal and benefit from:

- ▶ Convenient online submission
- ▶ Rigorous peer review
- ▶ Open access: articles freely available online
- ▶ High visibility within the field
- ▶ Retaining the copyright to your article

Submit your next manuscript at ▶ [springeropen.com](https://www.springeropen.com)
